ANALYSIS AND SIMULATION OF NEAR-FIELD WAVE MOTION DATA FROM THE SOURCE PHYSICS EXPERIMENT EXPLOSIONS

Tarabay H. Antoun, Heming Xu, Oleg Y. Vorobiev, Eric B Herbold, Lew A. Glenn, and Ilya N. Lomov

Lawrence Livermore National Laboratory

Sponsored by the National Nuclear Security Administration

Award No. DE-AC52-06NA25946/NST11-NCNS-TM-EXP-PD15

ABSTRACT

The Source Physics Experiment (SPE-N) at the Nevada National Security Site is planned as a series of chemical explosions under a variety of emplacement conditions. The goal of the SPE-N is to improve our physical understanding and ability to model explosively generated seismic waves, particularly S-waves. The first SPE explosion (SPE1) consisted of a 100 kg shot at a depth of 60 meters in granite (Climax Stock). The shot was well-recorded by an array of over 150 instruments, including both near-field wave motion measurements as well as far-field seismic measurements. This paper focuses on measurements and modeling of the near-field data. A complimentary study focusing on far-field seismic observations is the subject of a companion paper (Mellors et al., these Proceedings). The near-field data included triaxial acceleration measurements at eighteen different locations azimuthally distributed around the explosive charge. Three triaxial accelerometers were embedded in each of six vertical boreholes, distributed in two concentric rings around the charge. The inner ring consisted of three equidistant boreholes at a radius of 10 m from the charge, and the outer ring consisted of another three equidistant boreholes at a radius of 20 m. In each borehole, the accelerometers were vertically distributed at depths of 60 m (shot horizon), 50 m and 15 m. Surface accelerations were also recorded along a radial line centered at surface ground zero. A review of the SPE1 data shows that the peak radial velocity as a function of scaled range is consistent with previous nuclear explosion data but exhibits greater variability. The scaled peak radial displacement variation also exhibits greater variability but the mean values are significantly higher than exhibited in previous nuclear explosion data. These higher displacements were also observed in calculations performed with an ensemble constitutive model, which was based on nuclear explosion data in hard rock, but employed a Jones-Wilkins-Lee (JWL) equation of state for the ammonium nitrate fuel oil (ANFO) explosive mix used in SPE1. The reason for this behavior is believed to be the higher effective ratio of specific heats in the explosion products of the chemical explosive, leading to higher residual cavity pressure. Azimuthal scatter in the velocity data correspond to joint orientation, and as anticipated, the joints appear to be the principal source of observed shear wave generation in the near-field. Preliminary modeling of the SPE1 data shows that continuum simulations that do not explicitly account for the effect of joints will not successfully reproduce the observed directional variations in the recorded data. However, 2D and 3D simulations that explicitly account for joints and pre-existing fractures show that a low friction angle, derived with water-filled joints, may account for the observed variation in peak velocity and displacement. Waves appear to propagate more readily in the direction of persistent joints, as opposed to staggered joints. Furthermore, the anisotropy associated with wave propagation seems to be more pronounced when the friction angle was lowered to account for the effect of saturation. Further modeling will be conducted with continued focus on the effect of the presence of joints and their properties on shear wave generation. Simulation results will be compared to experimental measurements of both radial and non-radial motions from the SPE1 event, as well as from planned future SPE explosions.

Note: The Source Physics Experiments at the Nevada Nuclear Security Site (SPE-N) in 2011 should not be confused with the 2003 Source Phenomenology Experiments conducted in Arizona (SPE-A) (Yang and Bonner, 2009).

OBJECTIVES

The SPE-N is planned as a series of chemical explosions under a variety of emplacement conditions. The SPE-N goal is to improve our physical understanding and ability to model how explosions generate seismic waves, particularly S-waves.

RESEARCH ACCOMPLISHED

Continuum Modeling

An Eulerian hydrocode, GEODYN, was used to calculate spherical wave propagation both in 2D and 3D. The (ensemble) constitutive model employed was calibrated to match peak velocities and displacements for a number of underground nuclear explosions of different magnitude in granitic rock conducted both in the US and abroad (Antoun et al., 2002).

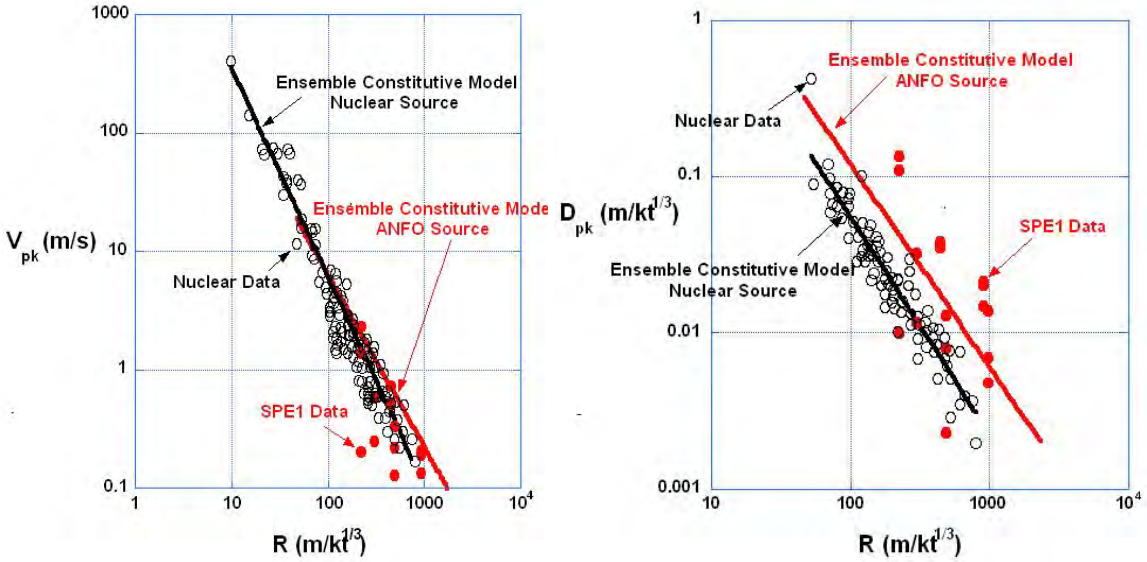

Figure 1. Peak velocity and displacement calculated with the ensemble model compared with SPE1 data. The black lines are least squares power-law fits to the ensemble constitutive model with nuclear source and the red lines are least squares power-law fits to the ensemble model with SPE-N ANFO source.

Figure 1 shows that there is only a slight difference between the calculated velocity attenuation with nuclear or chemical sources and both represent the SPE1 data reasonably well; though the latter exhibit considerable scatter. On the other hand, the calculated displacement is higher by roughly a factor of 2 for an ANFO explosion compared to a nuclear explosion of the same yield. This trend is also exhibited by the measured data. The reason for this behavior is believed to be the higher effective ratio of specific heats in the explosion products of the chemical explosive, leading to higher residual cavity pressure (Glenn and Goldstein, 1994).

The ensemble model is an isotropic plasticity model designed for large scale simulations. It does not use small scale test data for calibration and assumes that any joints in the granite formation are distributed uniformly resulting in an isotropic material response. Since the model is isotropic, it cannot explain the observed variability in the data, deviations from spherical wave propagation or the generation of significant shear (transverse) waves from explosions. However, even the closest gage location at 10 m indicates the wave motion data from SPE1 exhibits significant non-radial motions. These non-radial motions are not symmetrically distributed around the source, and like the radial motions, they exhibit significant azimuthal variations. Data from the instrumentation bore holes, as well as from the SPE1 charge emplacement hole indicate that the granite is highly fractured, with an average joint spacing of about 1ft (30.5 cm). In addition, the data shows that the joints are not randomly oriented; instead, four joint sets have been identified; each of which exhibit a distinct orientation with relatively little variability. The high

angle joint sets identified from the data are shown in Figure 2(a). Figure 2(b) is a graphic depiction of the peak radial velocities recorded at all gage locations in the SPE1 near-field. The vectors shown are oriented in the direction of the sensor and their magnitudes are proportional to the magnitude of the measured peak radial velocity. For ease of presentation, they have all been aggregated around the circumference of a circle centered on the charge. This figure appears to show a correlation between the orientation of the joints and the preferential directions of energy radiation. Even though this correlation is not conclusive due to the loss of data at some of the gage stations, it is sufficiently compelling to advance the hypothesis that the rock fabric, as manifested by the joints and fractures, is primarily responsible for the observed non-radial motions as well as the azimuthal variations in the near-field motion measurements. The remainder of this paper will examine this hypothesis utilizing detailed mesoscale simulations that discretely incorporate the joints and account for slip along their surfaces.

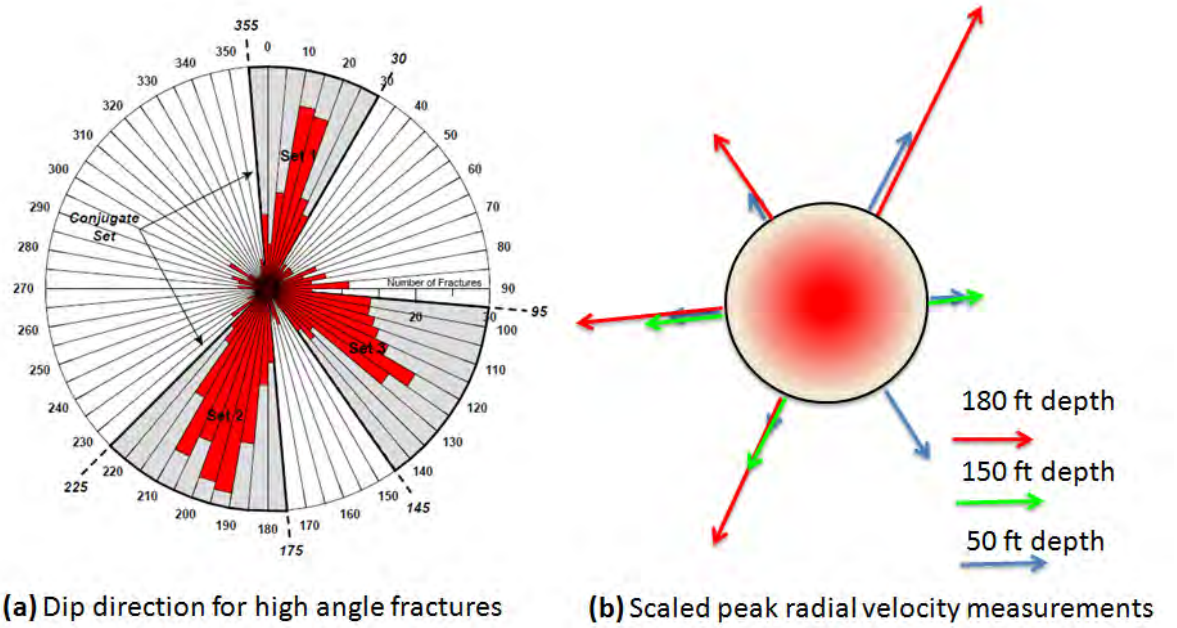

Figure 2. Correlation between the orientation of the joint sets in the SPE1 test bed (a) and the radial motions recorded at all the near-field sensor locations.

Discrete Modeling

In the discrete mesoscale simulations, the geologic medium is represented as an assembly of intact rock blocks separated by joints and fractures. The intact rock is modeled using a constitutive model that accounts for the salient features of the response of geologic materials, and calibrated for granite using laboratory data, including data from core samples obtained from the SPE1 test bed. The joints are modeled as frictional interfaces with their own constitutive relations, which include governing equations for both frictional sliding along the joint surface as well as compressibility, or compliance, normal to the joint surface. The computational resources required in this case are formidable because of the large number of joints and the 3D character of the problem. Preliminary analysis done in 2D showed that the joint orientation and persistence play a big role in formation and attenuation of the waves (see Figure 3).

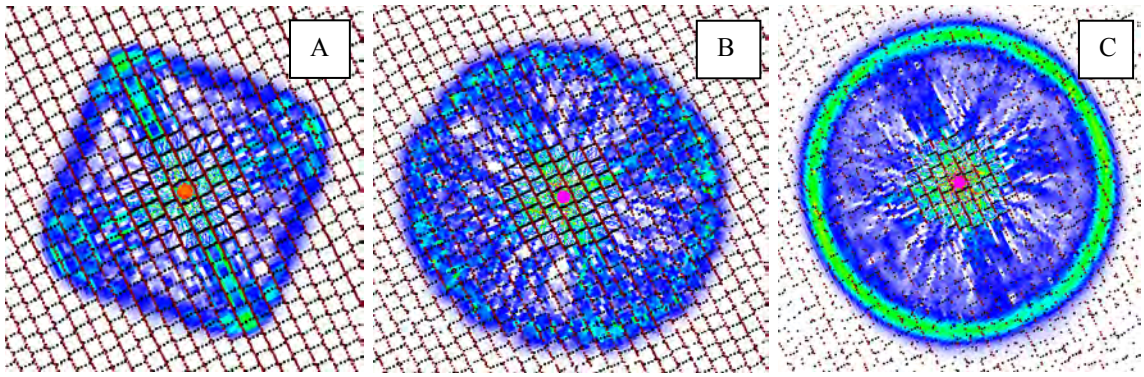

Figure 3. Pressure contours (0-200 MPa) calculated in a 2–set joint system with different persistency (A-100%, B-75% and C-25%).

By decreasing the joint persistency from 100% (Figure 3(a)) to below 75% (Figure 3(b) and (c)) an anisotropic wave becomes a symmetric wave that would be generated in an isotropic media.

For the SPE1 calibration shot, we used a Lagrangian hydrocode, GEODYN-L (Vorobiev, 2010) to model 3D wave propagation in a region 100x100x100 m with two joint spacings, 3 m and 1.5 m to study the effect of joints on the wave propagation.

Granite Model for Small Samples and its Extension to Large Scale

The model developed in (Liu et. al., 2005; Vorobiev et. al., 2007; Vorobiev, 2008) was used to describe the constitutive behavior of the intact granite. It describes the effects of bulking, porous compaction, shear enhanced compaction, and pressure dependent yield on the material response. The yield strength function is chosen in the form

$$Y = Y_{HB} F(\beta)\left[\delta + (1-\delta)\left(\frac{P_c - \max(P_0, P^*)}{P_c - P_0}\right)^r\right] R(\dot{\varepsilon}),$$

$$Y_{HB} = Y_c\left[\sqrt{s + \frac{m^2}{36} + \frac{mP^*}{Y_c}} - \frac{m}{6}\right], \qquad (1)$$

$$0 < \delta = \frac{\varepsilon_p}{\varepsilon_{p0} + \varepsilon_p} < 1,\ r > 1,\ P^* = P / R(\dot{\varepsilon}),$$

where β is the Lode angle, Y_c is the unconfined compressive strength, δ is a function of plastic strain describing material hardening, P_c and P_0 are history dependent variables describing a cap surface that governs porous compaction and Y_{HB} is the ultimate compressive strength. The coefficients *s* and *m* depend on the quality of the rock as expressed by the Geological Strength Index (GSI), a rock quality index widely used by the geotechnical engineering community:

$$s = \exp\left(\frac{GSI - 100}{9}\right),\ m = m_i \exp\left(\frac{GSI - 100}{28}\right) \qquad (2)$$

For the intact material, *s*=1 and the value m_i can be found from static laboratory tests on intact samples.

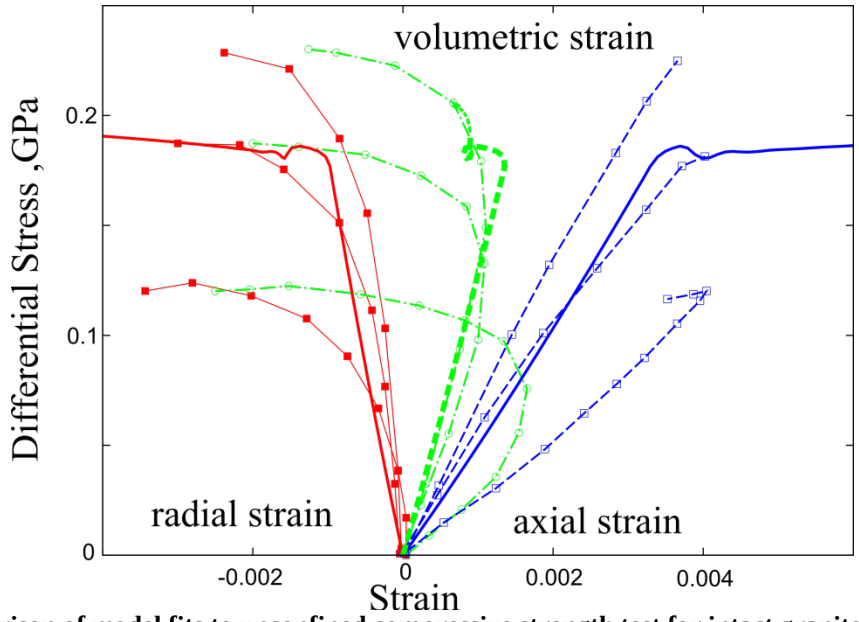

Figure 4. Comparison of model fits to unconfined compressive strength test for intact granite samples from the SPE-N test bed. Bold lines are simulation results, and thinner lines with markers are experimental data (Broome, 2011).

The model described by Equations (1) and (2) was calibrated to match intact granite data from the literature, as well as the unconfined compressive tests performed on the granite samples collected at the SPE1 site (see Figure 4). The model can be scaled to field scale by changing the GSI index, introducing extra porosity associated with the joints and modifying the porous compaction law. Figure 5 shows, that while the small scale model does not reproduce the wave attenuation data for large scale explosions, such as SPE1, it can be tuned to match the data by changing the GSI index, which describes the quality of rock mass. In this case, a GSI=60 was needed to match the measured displacement, which appropriately corresponds to a blocky rock with fair-to-poor surface conditions. In the mesoscale simulations described below, we used the model for intact granite, because the joints are included explicitly in the simulations.

Model for Dry and Wet Joints Informed by Meso-scale Modeling

One complicating factor in performing the discrete mesoscale simulations described here is the lack of joint characterization data to calibrate the contact parameters used in the simulations. This is further exacerbated by the presence of a perched water table at the location of the SPE1 shot, thus introducing added complications to the behavior of the joints. To alleviate this shortcoming, and provide the information needed for a reasonable representation of the response of the joints in the mesoscale simulations, a series of detailed simulations were performed to examine the behavior of a single joint under both dry and saturated conditions. Hydrocode simulations are performed here with GEODYN, which is a massively parallel Eulerian hydrocode with AMR capabilities. The "synthetic data" obtained from the single joint simulations were used to calibrate the joint model utilized in the mesoscale simulations of the SPE1 near-field.

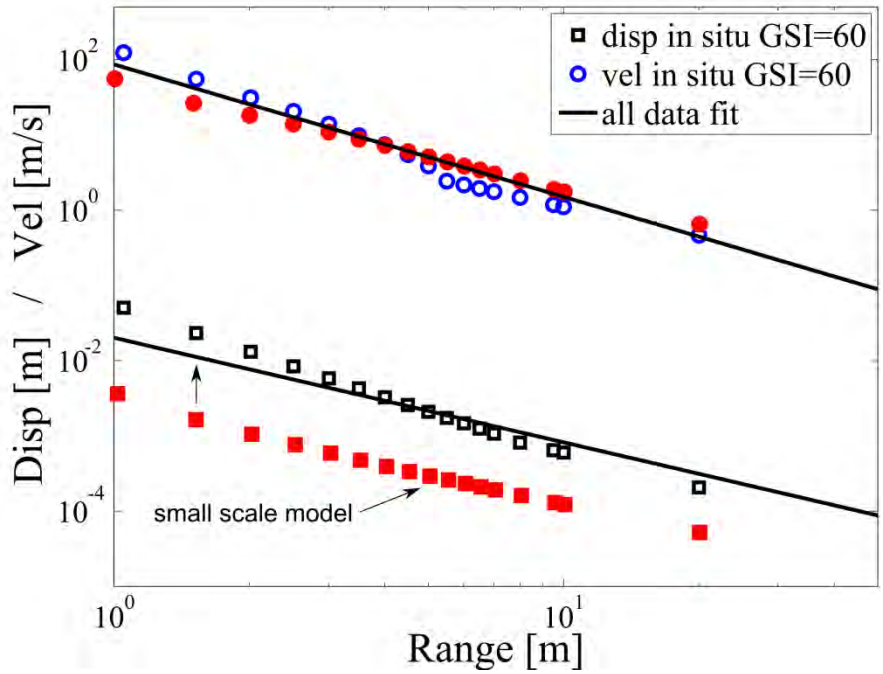

Figure 5. Peak displacement and velocity attenuations calculated in 1D spherical explosion using the small scale model (solid squares and circles) versus the nuclear data fit. Open squares and circles show an *in situ* model calculation.

The maximum shear strength of a rock joint depends on the normal stress. Coulomb's linear relationship describes this dependence well within the range of experimental data:

$$\tau = c + \sigma_n \tan\phi \tag{3}$$

where τ is the peak shear stress σ_n is the normal stress, c is the cohesion intercept and ϕ is the friction angle. It is assumed that these stresses are averaged along the length of the crack. A wider ranging empirical model was introduced by Barton to predict the maximum possible shear for a given applied normal stress that accounts for curvature in the strength envelopes for non-planar rock joints (Barton, 1973; Barton and Choubey, 1977). Barton introduces the joint roughness coefficient (*JRC*), the joint compressive strength (*JCS*) and a basic friction angle (ϕ_b) in his model, which have made it quite popular due to the simple determination of these parameters. For example, the *JRC* is determined by visual inspection. In this section we characterize the roughness of a simulated joint using the ideas from Barton and compare a dry and wet joint for the granite at the SPE1 site.

To characterize the joint we simulate a joint surface with a specific roughness that is correlated to the commonly used *JRC* values. The successive random midpoint method is used to perturb a 500 mm line as shown in Figure 6. To objectively quantify the *JRC* value, the fractal dimension must be related through an empirical expression (Lee et. al., 1990):

$$JRC = -0.87804 + 37.7844\left(\frac{D-1}{0.015}\right) - 16.9304\left(\frac{D-1}{0.015}\right)^2 \tag{4}$$

where D is the fractal dimension. The fractal dimension of the line shown in Figure 6 is $D = 1.00548$ which corresponds to $JRC = 11$ from Equation (4).

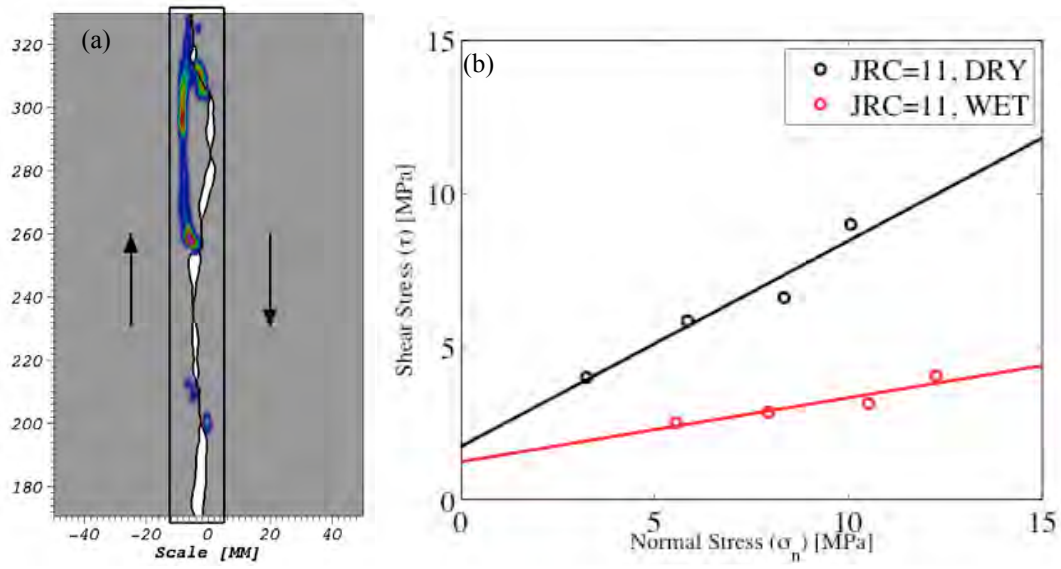

Figure 6. GEODYN simulation and results. (a) Part of the 500 mm long joint profile is shown at left with damage indicated by the color overlay. The left side of the fractal joint is moving upward at 5 m/s and the right is moving downward with the same speed. At the end of the simulation the stresses in each vertical slice from the boxed region are integrated for every time step. (b) The integrated normal and shear stress pairs with a least squares fit to Equation (3).

Figure 6 shows the results for 8 different simulations for a dry and wet joint with a mid-range roughness coefficient (JRC=11). The left side of the fractal joint is moving upward at 5 m/s and the right is moving downward with the same speed. Initially, a linear vertical velocity gradient is specified across the joint. The initial gap between the two matched surfaces is 2.5 mm. At the end of the simulation the stresses in each vertical slice from the boxed region are integrated for every time step. The integrated normal and shear stress pairs are shown in Figure 6(b) and the maximum shear stress is determined and plotted in the figure at right. A least squares fit of this data produces the cohesion and averaged friction coefficient (see Equation 3) for the velocity range detected at 10 m distance in the SPE1 experiment. The values for the black and red line in the figure corresponding to the two terms in Equation (3) are: (dry) c =1.74, tan(ϕ)=0.67, (wet) c =1.24, tan(ϕ)=0.21.

Discrete Problem Setup

The jointed rock formation was created by paving the space with parallelepiped blocks. Each block was subdiscretized by a number of elements with contacts set at the exterior faces. The properties of the contacts were varied randomly from sticky to weak contact (with low frictional coefficient, corresponding to the wet joint described above). In addition to the frictional properties, the persistence of the joints was controlled by staggering the blocks in two directions. This approach allowed us to describe a joint system with three main joint directions. These directions were identified from the experimental characterization of the joints at different locations. Figure 7 displays the 3D problem setup and Figure 8 shows the measured joint dip directions, as well as the orientation of the XY plane, used in the calculations. The X axis was oriented with joint set #1 (see Figure 2(a) for joint set definition). Note that we have treated the two closely oriented joint sets #1 and #2 from Figure 2(a) and Figure 8 as a one joint set #1 in the simulations as indicated by the red arrow in Figure 7 (a).

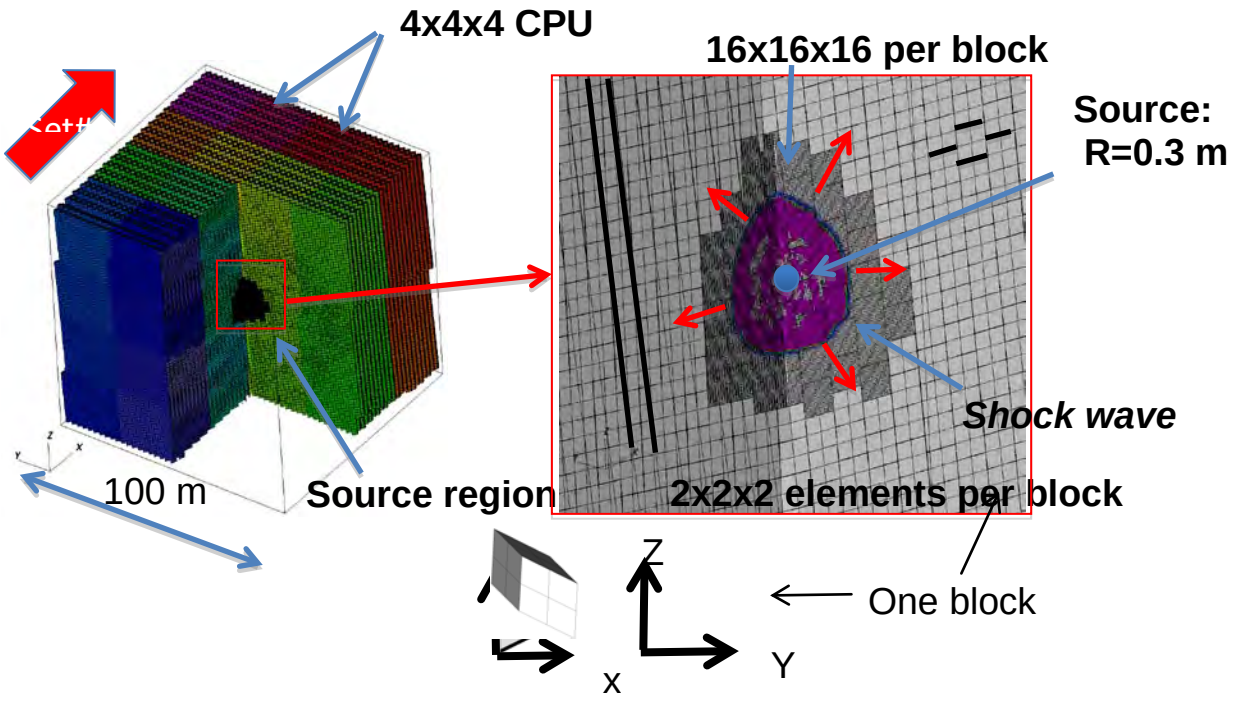

Figure 7. 3D problem initialization for rock formation with 3 joint sets. The Z axis is oriented towards the surface. The blocks around the source (at depth Z=-55 m) were further refined.

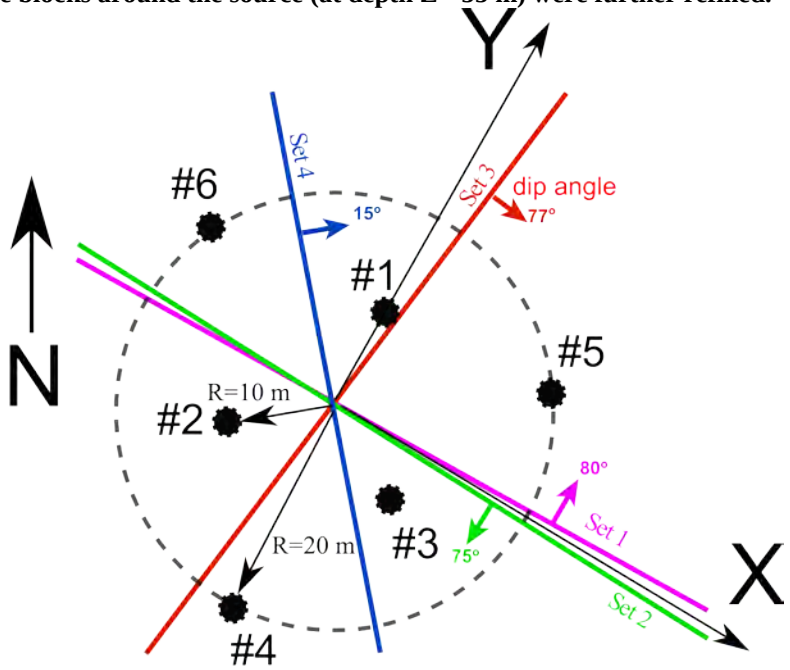

Figure 8. Joint dip directions, well locations and coordinate axis locations.

Simulation results

The results of our discrete simulations indicate that joints may induce a large amount of anisotropy. Figure 9 shows that there is a significant variation in attenuation of radial velocity in the horizontal plane at 180 ft (explosion depth) at ranges of 10 and 20 m and at ranges of 14 m and 22 m at a depth of 150 ft (10 m above). This can be explained by

sliding that occurs at the joints and is confirmed by the discrete calculations. Both the discrete calculations performed with GEODYN-L and the experiments show significant scatter in peak velocity and peak displacement values measured at the same range at different azimuths, which indicates that the joints have a profound effect on the wave anisotropy and can help explain the experimental observations. Figure 10 shows radial velocity histories calculated at two ranges, 10 m and 20 m. As in the experiment, the peak velocities are different at various azimuths. The velocities shown in Figure 10 correspond to X and Y directions, which are the most favorable for wave propagation. Similar to the calculations, the highest velocity was measured at location #1, which is shown with the solid line. Results of the simulations underestimate both the velocity and displacement at location #1. This is likely due to the fact that we have used roughly 3 times larger joint spacing than extant from observations. The calculation cost increases rapidly with the number of joints treated by the contacts and there were insufficient resources available in our preliminary study. Code improvements are underway to enable more realistic simulations that utilize the actual joint spacing. Preliminary results indicate that both peak velocity and the displacement should increase when more joints are added. Moreover, the results show that taking the joints into consideration dramatically changes the wave forms.

The calculations shown in Figure 10 were done with the intact model without joints (GEODYN), as well as with the jointed model (GEODYN-L). The GEODYN calculations produced peak velocities a factor of 2, and peak displacements ~20 times, smaller than those observed in the SPE1 experiment, whereas the GEODYN-L simulations that included the joints produced results that are comparable to the data, once again highlighting the important role that the rock fabric plays in shaping the waves produced by subsurface explosions.

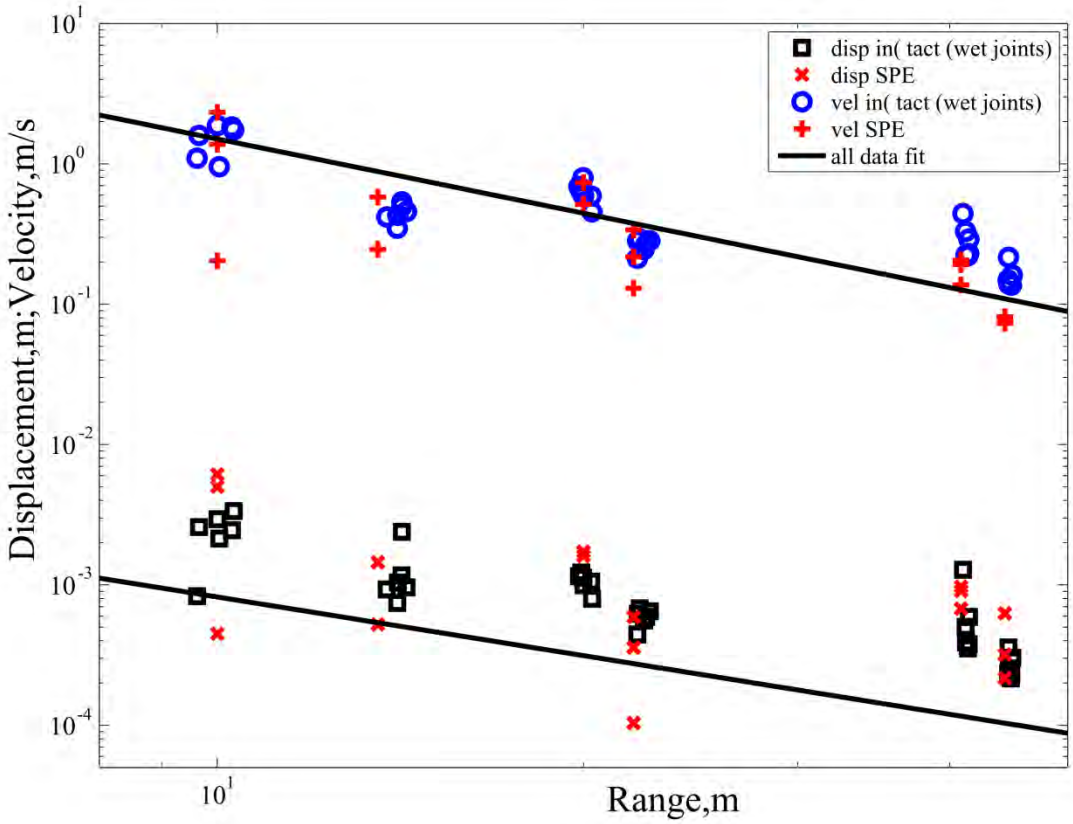

Figure 9. Peak velocity and displacement versus range measured in experiment (crosses) and calculated using discrete model (circles and squares). The solid line shows the nuclear explosion data fit.

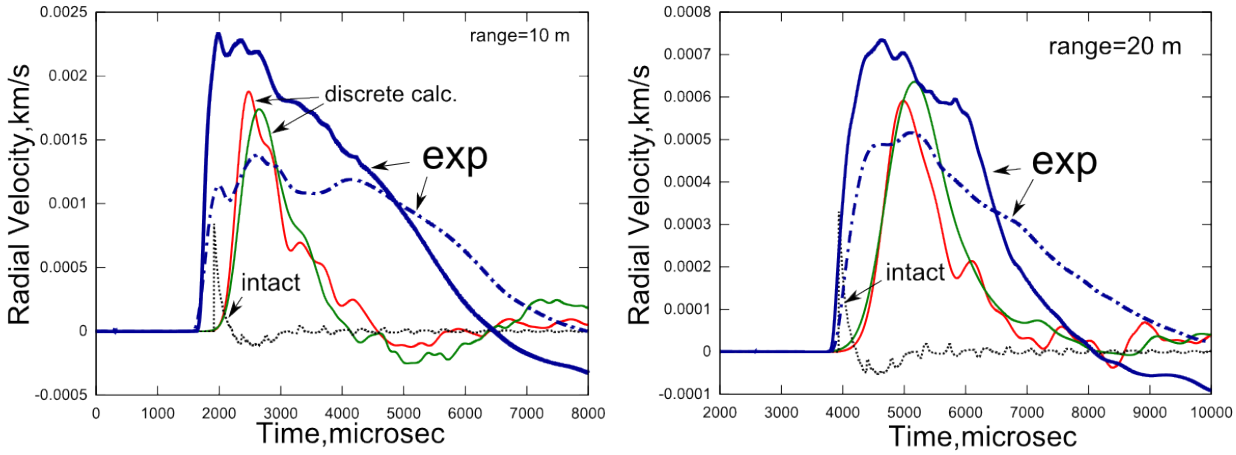

Figure 10. Radial velocity evolution measured in experiments and calculated with discrete modeling (green and red curves) using 1.5 m joint spacing and 12 degree friction angle at two different ranges, 10 m and 20 m. Comparison is also made with continuum calculations with the intact model without joints.

CONCLUSIONS AND RECOMMENDATIONS

Results from SPE1 show peak radial velocity as a function of scaled range is consistent with previous nuclear explosion data but exhibits somewhat greater variability. The scaled peak radial displacement variation also exhibits greater variability but the mean values are significantly higher than exhibited in previous nuclear explosion data. The reason for the larger displacements is believed to be the higher effective ratio of specific heats in the explosion products of the chemical explosive, leading to higher residual cavity pressure. Preliminary 2D and 3D calculations suggest that the observed variations in both peak velocity and displacement can be explained by the presence of water-filled joints. We have shown that using discrete simulations, where joints in the rock formation are treated explicitly, helps to understand the anisotropy in wave propagation. The simulated velocity and displacement histories were sensitive to average joint spacing, statistical variation in joint spacing, and joint persistency. Site specific information on these joint properties would better constrain the models and improve the quality of the results.

Finally, it should be noted that in the discrete simulations we used a constitutive model for the rock that was obtained by calibration with laboratory-scale rock samples collected from the site which is in contrast to traditional approaches where laboratory-scale data are arbitrarily modified to fit field-scale results.

REFERENCES

Antoun, T. H., Lomov, I. N., and L. A. Glenn (2001). Development and Application of a Strength and Damage Model for Rock under Dynamic Loading, *Proceedings of the 38th U.S. Rock Mechanics Symposium, Rock Mechanics in the National Interest*, Edited by D. Elsworth, J. Tinucci, and K. Heasley, A.A. Balkema Publishers, Lisse, The Netherlands, 369–374.

Barton,N. (1973). Review of a New Shear-Strength Criterion for Rock Joints, *Engineering Geology* **7**, 287-332.

Barton, N. and V. Choubey (1977). The Shear Strength of Rock Joints in Theory and Practice, *Rock Mechanics Felsmechanik Mecanique Des Roches,* 10: 1–54.

Broome, S., and T. Pfeifle (2011). Phase 1 Mechanical Testing Results on Core from Borehole U-15n, Nevada National Security Site, in Support of NCNS Source Physics Experiment, Technical Memo 6914, Sandia National Laboratories, June 8.

Coulson, J. H. (1971). *Proceedings of the 13th Symposium On Rock Mechanics*, edited by E.J. Cording (Urbana, Ill, 1971): 77–105.

Glenn, L. A. and P. Goldstein (1994). *J. Geophys. Res.* 99 (B6): 11723–11730.

Lee,Y., J. Carr, D. Barr, and C. Haas (1990). The Fractal Dimension as a Measure of the Roughness of Rock Discontinuity Profiles, *Int. J. Rock Mech. Min. Sci. Geomech. Abstr.,* 27: 453–464.

Liu, B. T., Lomov, I., and Vorobiev, O. (2005). Simulation of Shock Loading in Saturated Geologic Materials, in *Proceedings of the International Symposium on Plasticity*.

Mellors, R., A. Rodgers, P. Harben, W. Walter, S. Ford, J. Wagoner, A. Petersson, B. Sjogreen T. Hauk, S. Ruppert, S. Myers, E. Matzel, D. Dodge, M. Pasyanos, and J. Lewis (2011). Analysis and simulation of far-field seismic data from the Source Physics Experiment explosions, these Proceedings.

Vorobiev, O. (2008). Generic strength model for dry jointed rock masses. *Int. J. Plast.* 24(12): 2221–2247.

Vorobiev, O. Y., Liu, B. T., Lomov, I. N., and T. H. Antoun (2007). Simulation of penetration into porous geologic media. *Int. J. Impact. Eng.* 34(4): 721–731.

Vorobiev, O. (2010). Discrete and continuum methods for numerical simulations of non-linear wave propagation in discontinuous media, *Int. J. Num. Meth. Engr.,* 482–507.

Yang, X. and J. L. Bonner (2009). Characteristics of chemical explosive sources from time-dependent moment tensors, *Bull. Seismol. Soc. Am*. 99: 1, 36–51.